Quasiparticle anisotropic hydrodynamics for central collisions

Mubarak Alqahtani, Mohammad Nopoush, and Michael Strickland

Phys. Rev. C **95**, 034906 — Published 10 March 2017

DOI: 10.1103/PhysRevC.95.034906

Quasiparticle anisotropic hydrodynamics for central collisions

Mubarak Alqahtani, Mohammad Nopoush, and Michael Strickland
Department of Physics, Kent State University, Kent, OH 44242 United States
(Dated: February 14, 2017)

We use quasiparticle anisotropic hydrodynamics to study an azimuthally-symmetric boost-invariant quark-gluon plasma including the effects of both shear and bulk viscosities. In quasiparticle anisotropic hydrodynamics, a single finite-temperature quasiparticle mass is introduced and fit to the lattice data in order to implement a realistic equation of state (EoS). We compare results obtained using the quasiparticle method with the standard method of imposing the EoS in anisotropic hydrodynamics and viscous hydrodynamics. Using these three methods, we extract the primordial particle spectra, total number of charged particles, and average transverse momentum for various values of the shear viscosity to entropy density ratio η/s. We find that the three methods agree well for small shear viscosity to entropy density ratio, η/s, but differ at large η/s, with the standard anisotropic EoS method showing suppressed production at low transverse-momentum compared to the other two methods considered. Finally, we demonstrate explicitly that, when using standard viscous hydrodynamics, the bulk-viscous correction can drive the primordial particle spectra negative at large p_T. Such a behavior is not seen in either anisotropic hydrodynamics approach, irrespective of the value of η/s.

PACS numbers: 12.38.Mh, 24.10.Nz, 25.75.-q, 51.10.+y, 52.27.Ny
Keywords: Quark-gluon plasma, Relativistic heavy-ion collisions, Anisotropic hydrodynamics, Equation of state, Quasiparticle model, Boltzmann equation

I. INTRODUCTION

Ultrarelativistic heavy-ion collision experiments at the Relativistic Heavy Ion Collider (RHIC) and the Large Hadron Collider (LHC) study the quark-gluon plasma (QGP) using high energy nuclear collisions. The collective behavior seen in these experiments is quite successfully described by relativistic fluid dynamics. In early works, relativistic ideal hydrodynamics was applied assuming the QGP to behave like a perfect fluid [1–3]. Later on, to include the dissipative (viscous) effects, viscous hydrodynamics has been applied [4–37]. Recently, due to the large momentum anisotropies generated during heavy-ion collisions, a new framework called anisotropic hydrodynamics has been developed [38–61] (for a recent review, see Ref. [62]). This new framework has been compared to traditional viscous hydrodynamics in many ways. For boost-invariant and transversely homogeneous systems, by comparing to exact solutions it has been shown that anisotropic hydrodynamics more accurately describes the dynamics in all cases considered [49, 54, 55, 63–65]. In addition, it has been shown that anisotropic hydrodynamics best reproduces exact solutions of Boltzmann equation subject to 1+1d Gubser flow [66–68]. Finally, we also mention that it has been shown that anisotropic hydrodynamics shows better agreement with data from ultracold Fermi gases experiments than viscous hydrodynamics [69, 70].

The anisotropic hydrodynamics program is now focused on making phenomenological predictions for heavy-ion physics, including anisotropic freeze-out and a realistic lattice-based equation of state (EoS) [57]. In a recent paper it was demonstrated how to impose a realistic EoS assuming approximate conformality of the QGP [57]. In Ref. [59] a different method for imposing a realistic EoS was proposed in which the non-conformality of the QGP is taken into account by modeling the QGP as a gas of massive quasiparticles with temperature-dependent masses. This quasiparticle approach is motivated by perturbative results such as hard thermal loop (HTL) resummation, where the quarks and gluons can have temperature-dependent masses [71–79]. In the quasiparticle anisotropic hydrodynamics framework one introduces a single-finite temperature mass which is fit to available lattice data for the QCD EoS. Once $m(T)$ is determined, the realistic EoS together with the non-equilibrium energy momentum tensor can be used to derive the dynamical equations for such a quasiparticle gas using Boltzmann equation [59]. In this work, we extend the previous 0+1d work of Ref. [59] to 1+1d and we also use "anisotropic Cooper-Frye freeze-out" to compute the primordial particle spectra [57]. We limit our considerations to 1+1d because full 2+1d or 3+1d simulations using the quasiparticle method would currently require large scale computational resources.

Here we compare results of quasiparticle anisotropic hydrodynamics to those obtained using the standard anisotropic hydrodynamics [57] and second-order viscous hydrodynamics. We will refer to the three methods considered herein as "aHydroQP", "aHydro" and "vHydro", respectively. For our calculations, we use the general 3+1d dynamical equations derived in our previous paper [59]. We solve the equations numerically and perform self-consistent hadronic freeze-out in order to compare the total number of charged particles N_{chg}, the average transverse momentum $\langle p_T \rangle$ for pions, kaons, and protons, and also their differential spectra predicted by each approach. We find that the three methods agree well for small shear viscosity to entropy density ratio, η/s, but differ at large η/s. We find, in particular, that when using standard viscous hydrodynamics, the bulk-viscous correction can drive the primordial particle spectra negative at large p_T. Such a behavior is not seen in either anisotropic hydrodynamics approach, irrespective of the value of η/s.

The structure of the paper is as follows. In Sec. II, two approaches used for implementing realistic EoS is explained. In Sec. III, dynamical equations for two anisotropic hydrodynamics methods are presented for azimuthally-symmetric boost-invariant systems. In Sec. IV we discuss anisotropic Cooper-Frye freeze-out in the context of leading-order anisotropic hydrodynamics. In Sec. V, our numerical results obtained using the three methods for central Pb-Pb and p-Pb collisions at LHC energies are presented. Sec. VI contains our conclusions and an outlook for the future. In App. A, we review the notation and conventions. App. B is about anisotropic distribution function used in the formulation. In App. C, we present details about second-order viscous hydrodynamics equations. Finally, all necessary identities and function definitions are collected in Apps. D and E.

II. EQUATION OF STATE

For the temperatures close to QCD phase transition, significant corrections to the Stefan-Boltzmann limit (ideal gas limit) are observed and, as the temperature decreases, the relevant degrees of freedom change from quarks and gluons to hadrons. The standard way to determine the QGP EoS is to use non-perturbative lattice QCD calculations. For this purpose, we use an analytic parameterization of lattice QCD data taken from the Wuppertal-Budapest collaboration [80]. We refer the reader to the Ref. [59] for more details. Herein we consider a system at finite temperature and zero chemical potential.

Method 1: Standard

In the "standard approach" for imposing a realistic EoS in anisotropic hydrodynamics, one exploits the conformal multiplicative factorization of the energy-momentum tensor components [38, 39] even though conformal system is explicitly broken. This approach is justified a priori by the smallness of corrections to factorization in the non-nonconformal case in the near-equilibrium limit [57]. For details concerning this method, we refer the reader to Ref. [57, 59].

Method 2: Quasiparticle

Since the standard method is only approximate, one needs an alternative implementation of the EoS which can be applied to non-conformal systems. In the quasiparticle EoS method, the QGP is taken to be gas of massive quasiparticles whose mass is temperature dependent. However, naive substitution of $m(T)$ into the thermodynamic relations obtained for constant-mass system would violate thermodynamic consistency [81]. As discussed before, thermodynamic consistency can be ensured by adding a temperature-dependent contribution to the energy-momentum tensor in equilibrium limit. Herein, we use the formalism developed in Ref. [59] which generalizes this idea to anisotropic hydrodynamics, in which case the mean-field contribution evolves as a non-equilibrium system parameter. For details concerning this approach, we refer readers to [59].

III. DYNAMICAL EQUATIONS

In what follows, the 1+1d anisotropic hydrodynamics equations for both quasiparticle and massless (standard) systems are presented [59]. The equations are based on moments of the Boltzmann equation for massive quasiparticles with a temperature-dependent mass. As a simplification, the collisional kernel is taken in the relaxation-time approximation. The derivations are based on an (ellipsoidally) anisotropic distribution function with a diagonal anisotropy tensor which includes the effect of bulk degree of freedom, Φ. Herein, $\alpha_i = (1+\xi_i+\Phi)^{-1/2}$ where ξ_i's are the diagonal momentum-space anisotropy parameters and λ is a temperature-like scale which represents the temperature only in the isotropic limit. For details, about the precise form of the distribution function and the various parameters, see App. B. Choosing two equations from the first moment, three from the second moment, together with the matching condition (which ensures the energy-momentum conservation), we end up with six equations for six independent variables $\boldsymbol{\alpha}$, λ, T, and $\theta_\perp$ as

$$D_u\mathcal{E} + \mathcal{E}\theta_u + \mathcal{P}_x D_x\theta_\perp + \frac{\mathcal{P}_y}{r}\sinh\theta_\perp + \frac{\mathcal{P}_z}{\tau}\cosh\theta_\perp = 0, \tag{1}$$

$$D_x\mathcal{P}_x + \mathcal{P}_x\theta_x + \mathcal{E}D_u\theta_\perp - \frac{\mathcal{P}_y}{r}\cosh\theta_\perp - \frac{\mathcal{P}_z}{\tau}\sinh\theta_\perp = 0, \tag{2}$$

$$\frac{D_u\mathcal{I}_x}{\mathcal{I}_x} + \theta_u + 2D_x\theta_\perp = \frac{1}{\tau_{\rm eq}}\left(\frac{\mathcal{I}_{\rm eq}}{\mathcal{I}_x} - 1\right), \tag{3}$$

$$\frac{D_u\mathcal{I}_y}{\mathcal{I}_y} + \theta_u + \frac{2}{r}\sinh\theta_\perp = \frac{1}{\tau_{\rm eq}}\left(\frac{\mathcal{I}_{\rm eq}}{\mathcal{I}_y} - 1\right), \tag{4}$$

$$\frac{D_u\mathcal{I}_z}{\mathcal{I}_z} + \theta_u + \frac{2}{\tau}\cosh\theta_\perp = \frac{1}{\tau_{\rm eq}}\left(\frac{\mathcal{I}_{\rm eq}}{\mathcal{I}_z} - 1\right), \tag{5}$$

$$\mathcal{E}_{\rm kinetic} = \mathcal{E}_{\rm kinetic,eq}\,, \tag{6}$$

where the derivatives D_α and divergences θ_α, with $\alpha \in \{u,x,y,z\}$, are defined in App. D.

Massive gas

For the system of massive quasiparticles one has

$$\mathcal{E} = \mathcal{H}_3(\boldsymbol{\alpha},\hat{m})\,\lambda^4 + B\,,$$

$$\mathcal{P}_i = \mathcal{H}_{3i}(\boldsymbol{\alpha},\hat{m})\,\lambda^4 - B\,,$$
$$\mathcal{I}_i = \alpha\,\alpha_i^2\,\mathcal{I}_{\rm eq}(\lambda,m); \qquad (i=x,y,z), \tag{7}$$

with $\mathcal{I}_{\rm eq}(\lambda,m) = 4\pi\tilde{N}\lambda^5\hat{m}^3K_3(\hat{m})$ and $\hat{m}\equiv m/\lambda$. As is discussed in [59], in order to find B one needs to integrate

$$\frac{dB_{\rm eq}}{dT} = -4\pi\tilde{N}m^2TK_1(\hat{m}_{\rm eq})\frac{dm}{dT}\,. \tag{8}$$

with $m(T)$ obtained from thermodynamics relation

$$\mathcal{E}_{\rm eq}+\mathcal{P}_{\rm eq} = T\mathcal{S}_{\rm eq} = 4\pi\tilde{N}T^4\,\hat{m}_{\rm eq}^3K_3\left(\hat{m}_{\rm eq}\right). \tag{9}$$

with the matching condition, $\mathcal{H}_3(\boldsymbol{\alpha},\hat{m})\lambda^4 = \mathcal{H}_{3,\rm eq}(\hat{m}_{\rm eq})T^4$ where $\hat{m}_{\rm eq} \equiv m/T$ and $\mathcal{H}_{3,\rm eq}(\hat{m}_{\rm eq}) \equiv \mathcal{H}_3(\mathbf{1},\hat{m}_{\rm eq})$.

Massless gas

The energy density and pressures in massless case are

$$\mathcal{E} = \mathcal{E}_{\rm eq}(\lambda)\,\hat{\mathcal{H}}_3(\boldsymbol{\alpha})\,,$$
$$\mathcal{P}_i = \mathcal{P}_{\rm eq}(\lambda)\,\hat{\mathcal{H}}_{3i}(\boldsymbol{\alpha})\,,$$
$$\mathcal{I}_i = \alpha\,\alpha_i^2\,\mathcal{I}_{\rm eq}(\lambda)\,; \qquad (i=x,y,z), \tag{10}$$

with $\mathcal{I}_{\rm eq}(\lambda) = 32\pi\tilde{N}\lambda^5$ and the matching condition $\mathcal{E}_{\rm eq}(\lambda)\hat{\mathcal{H}}_3(\boldsymbol{\alpha}) = \mathcal{E}_{\rm eq}(T)$.

IV. ANISOTROPIC FREEZE-OUT

At the late times, the system undergoes freeze-out procedure for particle production. For this purpose we perform "anisotropic Cooper-Frye freeze-out" using Eq. (B2) as the form for the one-particle distribution function. The advantage of this freeze-out method is that the anisotropic distribution function is guaranteed to be positive-definite, by construction, in all regions in phase space and the microscopic parameters can be taken directly from the aHydro evolution evaluated on the freeze-out hypersurface. In this paper, we follow the procedure derived in [57]; however, here we take into account the breaking of conformality. The only change required is in the argument of the distribution function itself, where the combination $p^\mu\Xi_{\mu\nu}p^\nu$ has additional terms associated with the bulk degree of freedom $\Phi = \frac{1}{3}\sum_i\alpha_i^{-2}-1$. Parameterizing the particle momentum in the lab frame as $p^\mu \equiv (m_\perp\cosh y, p_\perp\cos\varphi, p_\perp\sin\varphi, m_\perp\sinh y)$ where $m_\perp = \sqrt{p_\perp^2+m^2}$, $y=\tanh^{-1}(p^z/p^0)$ is the particle's rapidity, and φ is the particle's azimuthal angle, one obtains

$$\begin{aligned} p^\mu\Xi_{\mu\nu}p^\nu = {} & (1+\Phi)\Big[m_\perp\cosh\theta_\perp\cosh(y-\varsigma)-p_\perp\sinh\theta_\perp\cos(\phi-\varphi)\Big]^2 \\ & +\xi_x\Big[m_\perp\sinh\theta_\perp\cosh(y-\varsigma)-p_\perp\cosh\theta_\perp\cos(\phi-\varphi)\Big]^2 \\ & +\xi_y\,p_\perp^2\sin^2(\phi-\varphi)+\xi_z\,m_\perp^2\sinh^2(y-\varsigma)-\Phi m^2\,. \end{aligned} \tag{11}$$

Note that $p^\mu\Xi_{\mu\nu}p^\nu$ is Lorentz invariant, and by calculating it in LRF, one can show that this is positive definite in any frame.

V. RESULTS

We now turn to our numerical results. We present comparisons of results obtained using the dynamical equations of anisotropic hydrodynamics presented in Sec. III and the second-order viscous hydrodynamics equations from Denicol et al. [29, 33]. For details about the vHydro equations solved herein we refer the reader to App. C.

Pb-Pb collisions: For all results presented in this section we use smooth Glauber wounded-nucleon overlap to set the initial energy density. As our test case we consider Pb-Pb collisions with $\sqrt{s_{\rm NN}} = 2.76$ GeV. The inelastic nucleon-nucleon scattering cross-section is taken to be $\sigma_{\rm NN} = 62$ mb. For the aHydro results, we use 200 points in the radial direction with a lattice spacing of $\Delta r = 0.15$ fm and temporal step size of $\Delta\tau = 0.01$ fm/c. For the vHydro results, we use 600 points in the radial direction with a lattice spacing of $\Delta r = 0.05$ fm and temporal step size of $\Delta\tau = 0.001$ fm/c.[1] In all cases, we use fourth-order Runge-Kutta integration for the temporal updates and fourth-order centered differences for the evaluation of all spatial derivatives.[2] We take the central initial temperature to be $T_0 = 600$ MeV at $\tau_0 = 0.25$ fm/c and assume that the system is initially isotropic, i.e. $\alpha_x(\tau_0)=\alpha_y(\tau_0)=\alpha_z(\tau_0)=1$ for anisotropic hydrodynamics and $\pi^{\mu\nu}(\tau_0)=\Pi(\tau_0)=0$ for second-order viscous hydrodynamics. We take the freeze-out temperature to be $T_{\rm eff} = T_{\rm FO} = 150$ MeV in all cases

[1] We found that the vHydro code was more sensitive to the spatial lattice spacing and required a smaller temporal step size for stability.

[2] Since the initial conditions considered herein are smooth, naive centered differences generally suffice.

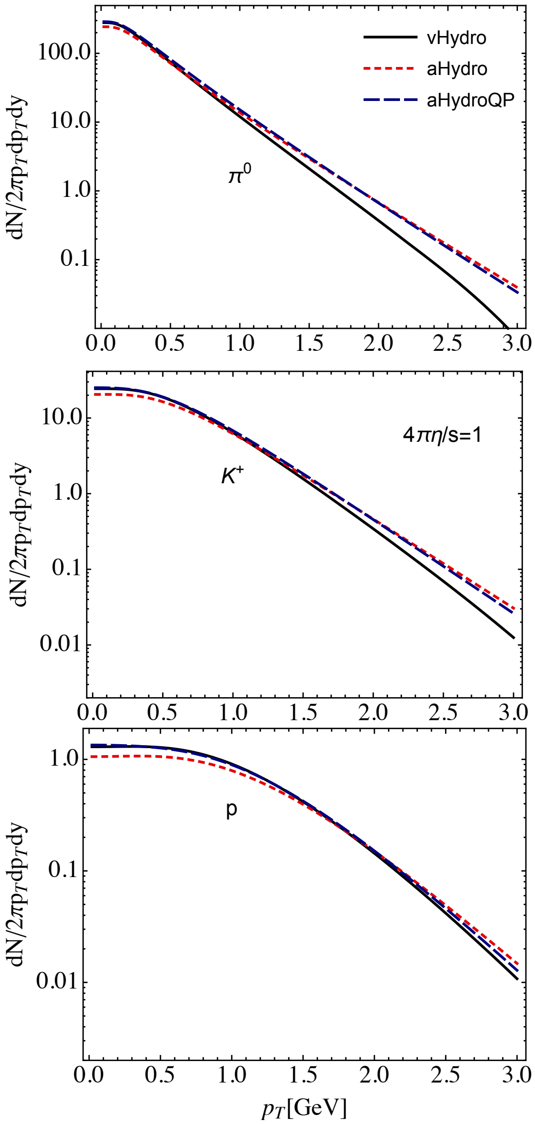

FIG. 1. Comparison of the neutral pions, kaons (K^+), and protons spectra as a function of transverse momentum p_T obtained using aHydroQP, aHydro and vHydro. The shear viscosity to entropy density ratio is $4\pi\eta/s = 1$.

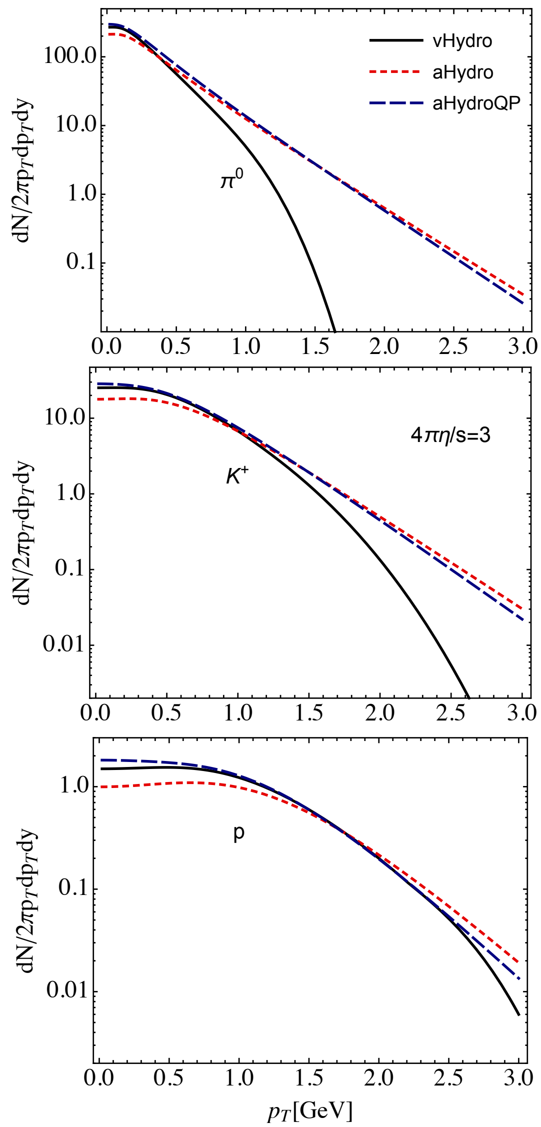

FIG. 2. Same as Fig. 1, except here the shear viscosity to entropy density ratio was taken to be $4\pi\eta/s = 3$.

shown. For the freeze-out we use 371 hadronic resonances ($M_{\rm hadron} \leq 2.6$ GeV), with the masses, spins, etc. taken from the SHARE table of hadronic resonances [82–84]. We do not perform resonance feed down, hence all spectrum shown herein are primordial spectra.

In Figs. 1-3 we present our results for the primordial pion, kaon, and proton spectra produced for $4\pi\eta/s = 1, 3$, and 10, respectively. In each case, we have held the initial conditions fixed and only varied η/s. In each of these figures the solid black line is the result from standard second-order viscous hydrodynamics (vHydro), the red short-dashed line is the result from standard anisotropic hydrodynamics (aHydro), and the blue long-dashed line is the result from quasiparticle anisotropic hydrodynamics (aHydroQP). As can be seen from Fig. 1, for $4\pi\eta/s = 1$, both aHydro approaches are in good agreement over the entire p_T range shown with the largest differences occurring at low momentum. The second-order viscous hydrodynamics result, however, shows a significant downward curvature in the pion spectrum resulting in many fewer high-p_T pions. The trend is the same for the kaon and proton spectra, however, for the larger mass hadrons the downturn is less severe. We note that although we plot only up to $p_T = 3$ GeV, these plots can be extended to larger p_T, in which case one finds that eventually the primordial pion spectrum predicted by vHydro becomes negative, which is clearly unphysical. This can be seen more clearly in Figs. 2 and 3 which show the same results for $4\pi\eta/s = 3$ and 10, respectively. As these figures demonstrate, for larger η/s the vHydro

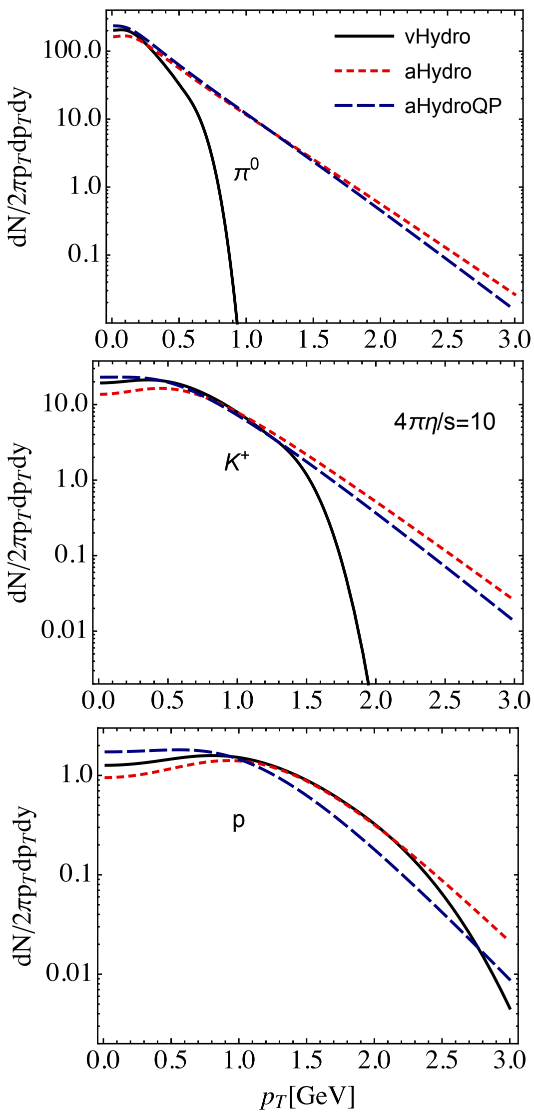

FIG. 3. Same as Fig. 1, except here the shear viscosity to entropy density ratio was taken to be $4\pi\eta/s = 10$.

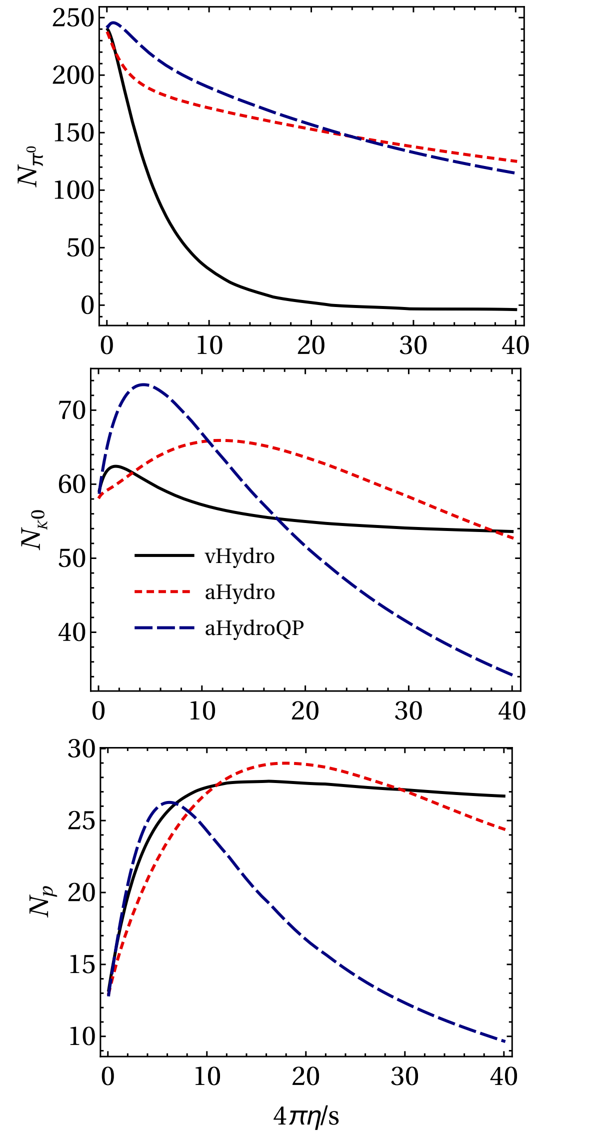

FIG. 4. Comparison of the total number of pions (π^0), kaons (K^0), and protons as a function of $4\pi\eta/s$ obtained using aHydroQP, aHydro, and vHydro.

primordial particle spectra become unphysical at lower momenta. For example, for $4\pi\eta/s = 3$ the differential pion spectrum goes negative at $p_T \sim 1.6$ GeV while for $4\pi\eta/s = 10$ it goes negative at $p_T \sim 0.9$ GeV.

This behavior is a result of the bulk-viscous correction to the one-particle distribution function specified in Eq. (C22). We have checked that if we neglect the bulk-viscous correction to the distribution function, then the resulting spectra are positive definite in the range of p_T shown in Figs. 1-3. We have verified that this is a known issue with the bulk-viscous correction in the second-order viscous hydrodynamics approach. The same form for the bulk correction (C22) was used by the authors of Ref. [35] and they also observed a downward curvature turning into negatively-valued spectra at large p_T [85]. This problem does not occur in either aHydro approach because the one-particle distribution function is positive-definite by construction in this framework.

Next, we turn to a discussion of Fig. 4. In this figure we plot the total number of π^0's (top), K^0's (middle), and p's (bottom) obtained by integrating the differential yields over transverse momentum as a function of $4\pi\eta/s$. The line styles are the same as in Figs. 1-3. From this figure we see that at small η/s all approaches are in agreement, however, at large η/s the three methods can give dramatically different results. We, in particular, note that the number of pions from vHydro drops much quicker than the two aHydro approaches. This is primarily due to the fact that in vHydro one sees a negative number of pions at large p_T. As shown in Fig. 4 (top), the total number of pions predicted by vHydro goes negative at $4\pi\eta/s \sim 22$. This is a signal of the breakdown of viscous hydrodynamics and should come as no surprise

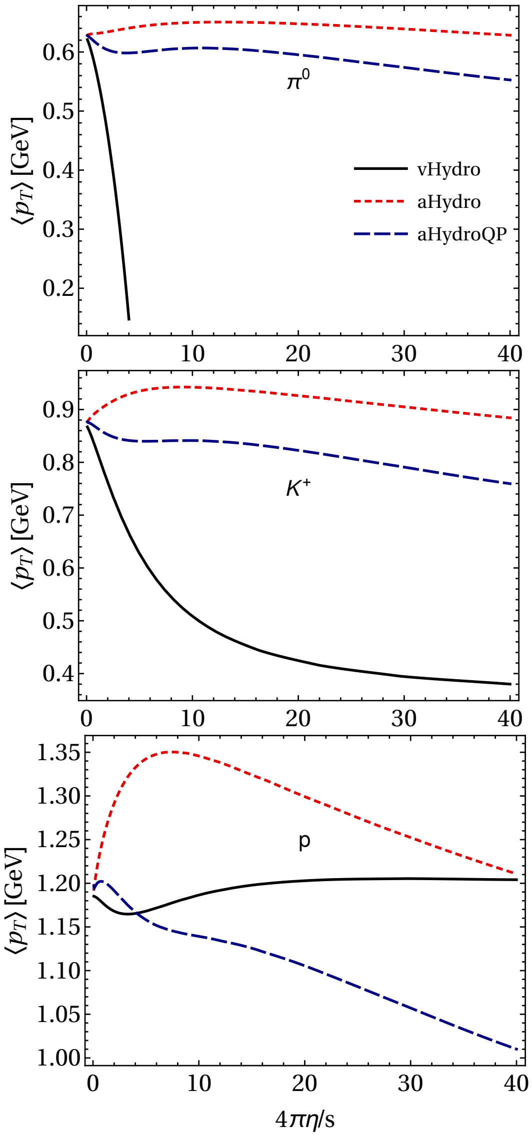

FIG. 5. Comparison of the neutral pions, kaons (K^+), and protons average transverse momentum as a function of $4\pi\eta/s$ obtained using aHydroQP, aHydro, and vHydro.

since this approach is intended to be applicable only in the case of small η/s and p_T. Finally, we note that although aHydro and aHydroQP are in reasonably good agreement for the pion and kaon spectra, we see a rather strong dependence on the way the EoS is implemented in the proton spectra and, hence, the total number of primordial protons.

As an additional way to compare the three methods considered, in Fig. 5 we present the average p_T for π^0's (top), K^+'s (middle), and p's (bottom). The line styles are the same as in Figs. 1-3. From this figure we see that both aHydro approaches predict a weak dependence of the pion and kaon $\langle p_T \rangle$ on the assumed value of η/s, whereas vHydro predicts a much more steep decrease in $\langle p_T \rangle$ for the pions and kaons. Once again, we see that the vHydro $\langle p_T \rangle$ for pions becomes negative for $4\pi\eta/s \gtrsim 5$. This rapid decrease stems directly from the negativity of the pion spectra at high p_T which is more important in this case since the integrand is more sensitive to the high-p_T part of the spectra. Finally, we note that once again the proton spectra and hence $\langle p_T \rangle$ for protons is sensitive to the way in which the EoS is implemented when comparing the two aHydro approaches.

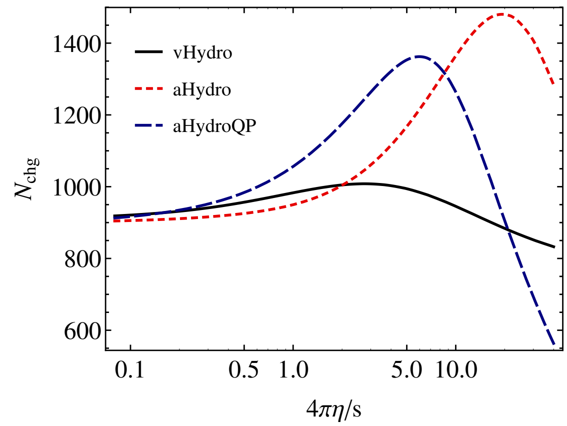

FIG. 6. The number of total charged particles as a function of $4\pi\eta/s$ obtained using aHydroQP, aHydro, and vHydro.

Finally, in Fig. 6 we plot the total number of charged particles as a function of $4\pi\eta/s$ predicted by each of the three approaches considered. Once again the line styles are the same as in Figs. 1-3. As this figure demonstrates, for small η/s all three frameworks are in agreement and approach the ideal result as η/s tends to zero. All three frameworks predict that $N_{\rm chg}$ at first increases, then reaches a maximum, and then begins to decrease. The precise turnover point depends on the method with the lowest turnover seen using vHydro around $4\pi\eta/s \sim 3$; however, this turnover is due in large part to the fact that the total pion number drops precipitously in vHydro.

p-Pb collisions: We now turn to the case of an asymmetric collision between a proton and a nucleus. For this purpose, we use the same parameters as used for the Pb-Pb collisions considered previously, except for p-Pb we use a lower initial temperature of $T_0 = 400$ MeV . In addition, for the aHydro results, we use a lattice spacing of $\Delta r = 0.06$ fm and for vHydro results, we use a lattice spacing of $\Delta r = 0.02$ fm. The smaller lattice spacings simply reflect the smaller system size of the QGP created in a p-Pb collision.

In Figs. 7-8 we present our results for the primordial pion, kaon, and proton spectra produced for $4\pi\eta/s = 1$, and 3, respectively in p-Pb collisions. As we can see from Fig. 7, both aHydro approaches are in a good agreement at high p_T, however, there are some quantitative differences at low p_T. Comparing the low p_T difference with that seen in Pb-Pb collisions, we find that there is a larger variation in the p-Pb spectra comparing aHydro and aHydroQP. This variation is a bit worrisome since it

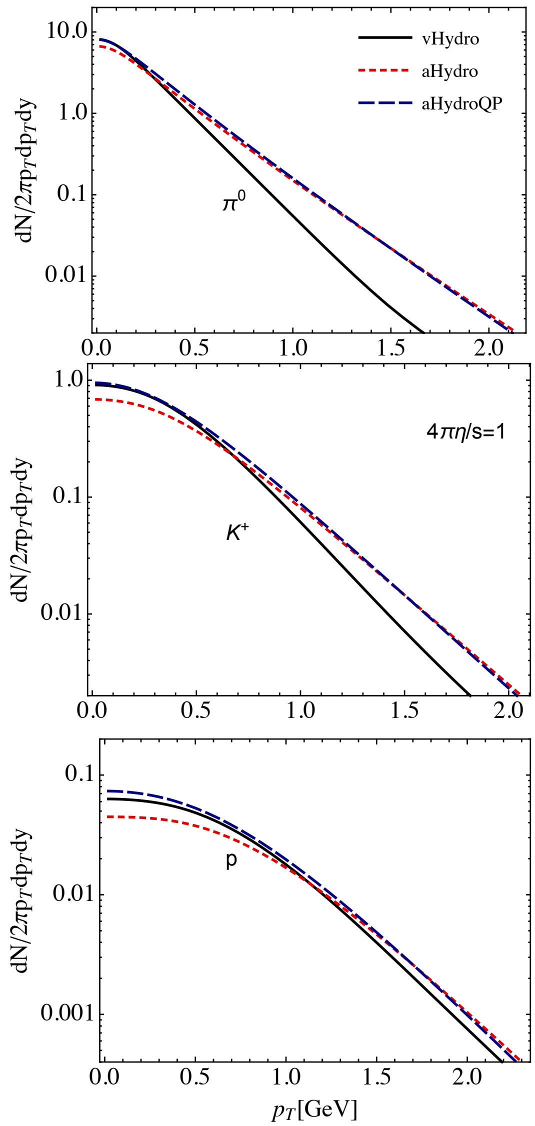

FIG. 7. Comparisons of the p-Pb neutral pions, kaons (K^+), and protons spectra as a function of transverse momentum p_T obtained using aHydroQP, aHydro, and vHydro. The shear viscosity to entropy density ratio is $4\pi\eta/s = 1$.

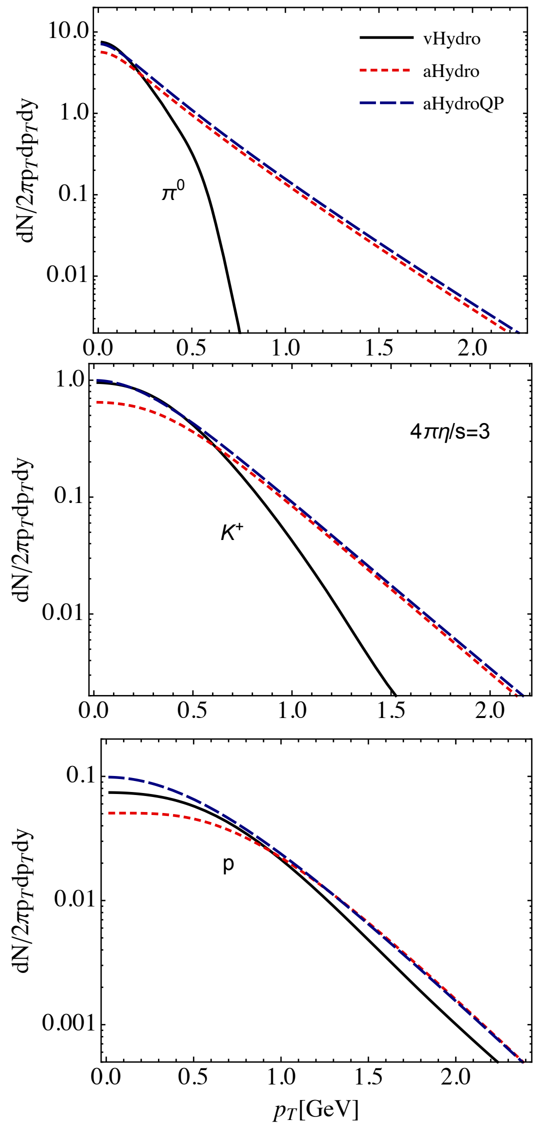

FIG. 8. Same as Fig. 7, except here the shear viscosity to entropy density ratio was taken to be $4\pi\eta/s = 3$.

indicates a kind of theoretical uncertainty in the aHydro approach. Importantly, however, we mention that the two aHydro results are quite different than the vHydro result. For p-Pb collisions, the vHydro result shows the same behavior seen in the Pb-Pb collisions, namely that the particle spectra goes negative at high p_T. In Fig. 8, one can clearly see the unphysical behavior in the vHydro primordial spectra. As a result, there is even larger theoretical uncertainty associated with applications of vHydro to p-Pb collisions.

VI. CONCLUSIONS AND OUTLOOK

In this paper, we compared three different viscous hydrodynamics approaches: aHydro, aHydroQP, and vHydro. For all three cases we included both shear and bulk-viscous effects using the relaxation time approximation scattering kernel. In the standard aHydro approach one uses the standard method for imposing an equation of state in anisotropic hydrodynamics, which is to obtain conformal equations and then break the conformality only when introducing the EoS itself. In aHydroQP, one takes into account the breaking of conformality at the outset by modeling the QGP as a quasiparticle gas with a single temperature-dependent mass $m(T)$ which is fit to available lattice data for the EoS. Finally, for our comparisons with viscous hydrodynamics we used the formalism of Denicol et al [29, 33] specialized to the case of relaxation time approximation.

For each method, we specialized to the case of 1+1d boost-invariant and azimuthally-symmetric collisions using smooth Glauber initial conditions. We specialized to this case because of the computational intensity of the aHydroQP approach which requires real-time evaluate of complicated multi-dimensional integrals which are functions of all three anisotropy parameters and the local temperature-dependent mass. Using the resulting numerical evolution, we then extracted fixed energy density freeze-out hypersurfaces in each case and implemented the scheme-appropriate freeze-out to hadrons allowing us to have an apples-to-apples comparison between the three different approaches. We found that the primordial particle spectra, total number of charged particles, and average transverse momentum predicted by the three methods agree well for small shear viscosity to entropy density ratio, η/s, but differ at large η/s. Finally we demonstrated that, when using standard viscous hydrodynamics, the bulk-viscous correction can drive the primordial particle spectra negative at large p_T. Such a behavior is not seen in either aHydro approach, irrespective of the value of η/s. Finally, and most importantly, we find a reasonable agreement between the two aHydro EoS implementations.

Looking to the future, it is feasible to extend the aHydroQP approach to 3+1d, however, this will be numerically intensive and require parallelization to implement fully. One possibility is to use polynomial fits to parametrize the various massive $\mathcal{H}$-functions necessary instead of evaluating them on-the-fly in the code. If this is possible, then aHydroQP could become a viable alternative to the standard method of implementing the EoS in aHydro and, since it takes into account the non-conformality of the system from the beginning, this could give us an idea of the theoretical uncertainty associated with the EoS method used in phenomenological applications. For now, this work will serve as a reference point for possible differences between the two approaches to imposing the aHydro EoS.

ACKNOWLEDGMENTS

We thank G. Denicol and B. Schenke for useful discussions. M. Strickland and M. Nopoush were supported by the U.S. Department of Energy, Office of Science, Office of Nuclear Physics under Awards No. DE-SC0013470. M. Alqahtani was supported by a PhD fellowship from the University of Dammam.

Appendix A: Conventions and Notation

In this section, we summarize the general conventions we used in the derivations. A parentheses in the indices indicates a symmetrized form, e.g. $A^{(\mu\nu)} \equiv (A^{\mu\nu} + A^{\nu\mu})/2$. The metric is taken to be in the "west coast convention" such that in Minkowski space with $x^\mu \equiv (t,x,y,z)$ the measure is $ds^2 = g_{\mu\nu}dx^\mu dx^\nu = dt^2 - dx^2 - dy^2 - dz^2$. We also use the standard transverse projector, $\Delta^{\mu\nu} \equiv g^{\mu\nu} - u^\mu u^\nu$. When studying relativistic heavy-ion collisions, it is convenient to transform to Milne coordinates defined by $\tau = \sqrt{t^2 - z^2}$, which is the longitudinal proper time, and $\varsigma = \tanh^{-1}(z/t)$, which is the longitudinal spacetime rapidity. For a system which is azimuthally symmetric with respect to the beam-line, it is convenient to transform to polar coordinates in the transverse plane with $r = \sqrt{x^2+y^2}$ and $\phi = \tan^{-1}(y/x)$. In this case, the new set of coordinates $x^\mu = (\tau, r, \phi, \varsigma)$ defines polar Milne coordinates. Also, $\tilde{N} \equiv N_{\rm dof}/(2\pi)^3$ with $N_{\rm dof}$ being the number of degrees of freedom.

Appendix B: Ellipsoidal distribution function

We introduce the anisotropy tensor in non-conformal anisotropic hydrodynamics as [44, 53]

$$\Xi^{\mu\nu} = u^\mu u^\nu + \xi^{\mu\nu} - \Delta^{\mu\nu}\Phi \,, \tag{B1}$$

where u^μ is four-velocity, $\xi^{\mu\nu}$ is a symmetric and traceless tensor, and Φ is associated with the bulk degree of freedom. The quantities u^μ, $\xi^{\mu\nu}$, and Φ are functions of spacetime and obey $u^\mu u_\mu = 1$, ${\xi^\mu}_\mu = 0$, ${\Delta^\mu}_\mu = 3$, and $u_\mu \xi^{\mu\nu} = 0$; therefore, one has ${\Xi^\mu}_\mu = 1 - 3\Phi$. The one-particle distribution function at leading order in the aHydro expansion is of the form

$$f(x,p) = f_{\rm iso}\left(\frac{1}{\lambda}\sqrt{p_\mu \Xi^{\mu\nu} p_\nu}\right), \tag{B2}$$

where λ has dimensions of energy and can be identified only with the temperature in the isotropic equilibrium limit ($\xi^{\mu\nu} = 0$ and $\Phi = 0$). Herein, we assume that the distribution function is of Boltzmann form and chemical potential is taken to be zero. To good approximation one can assume that $\xi^{\mu\nu} = {\rm diag}(0, \boldsymbol{\xi})$ with $\boldsymbol{\xi} \equiv (\xi_x, \xi_y, \xi_z)$ because the most important viscous corrections are to the diagonal components of $T^{\mu\nu}$. In this case, Eq. (B2) in the LRF gives

$$f(x,p) = f_{\rm eq}\left(\frac{1}{\lambda}\sqrt{\sum_i \frac{p_i^2}{\alpha_i^2} + m^2}\right), \tag{B3}$$

where $i \in \{x,y,z\}$ and the scale parameters α_i are

$$\alpha_i \equiv (1 + \xi_i + \Phi)^{-1/2} \,. \tag{B4}$$

For compactness, one can collect the three anisotropy parameters into vector $\boldsymbol{\alpha} \equiv (\alpha_x, \alpha_y, \alpha_z)$. In the isotropic equilibrium limit, where $\xi_i = \Phi = 0$ and $\alpha_i = 1$, one has

$p_\mu \Xi^{\mu\nu} p_\nu = E^2$ and $\lambda \to T$ and, hence,

$$f(x,p) = f_{\rm eq}\left(\frac{E}{T(x)}\right). \tag{B5}$$

Note that, out of the four anisotropy and bulk parameters there are only three independent ones. In practice, we use the three variables α_i as the dynamical anisotropy parameters since, by using Eq. (B4) and the tracelessness of $\xi^{\mu\nu}$, one can write Φ in terms of the anisotropy parameters, $\Phi = \frac{1}{3}\sum_i \alpha_i^{-2} - 1$.

Appendix C: Second-order viscous hydrodynamics

The second order viscous hydrodynamics equations including bulk viscosity are [29, 33]

$$(\mathcal{E}+\mathcal{P}+\Pi)D_u u^\mu = \nabla^\mu(\mathcal{P}+\Pi) - \Delta^\mu_\nu \nabla_\sigma \pi^{\nu\sigma} + \pi^{\mu\nu} D_u u_\nu\,, \tag{C1}$$

$$D_u \mathcal{E} = -(\mathcal{E}+\mathcal{P}+\Pi)\theta_u + \pi^{\mu\nu}\sigma_{\mu\nu}\,, \tag{C2}$$

$$\tau_\Pi D_u \Pi + \Pi = -\zeta\theta_u - \delta_{\Pi\Pi}\Pi\theta_u + \varphi_1 \Pi^2 + \lambda_{\Pi\pi}\pi^{\mu\nu}\sigma_{\mu\nu} + \varphi_3 \pi^{\mu\nu}\pi_{\mu\nu}\,, \tag{C3}$$

$$\tau_\pi \Delta^{\mu\nu}_{\alpha\beta} D_u \pi^{\alpha\beta} + \pi^{\mu\nu} = 2\eta\sigma^{\mu\nu} + 2\tau_\pi \pi_\alpha^{\langle\mu}\omega^{\nu\rangle\alpha} - \delta_{\pi\pi}\pi^{\mu\nu}\theta_u + \varphi_7 \pi_\alpha^{\langle\mu}\pi^{\nu\rangle\alpha} - \tau_{\pi\pi}\pi_\alpha^{\langle\mu}\sigma^{\nu\rangle\alpha} + \lambda_{\pi\Pi}\Pi\sigma^{\mu\nu} + \varphi_6 \Pi\pi^{\mu\nu}\,, \tag{C4}$$

where $\mathcal{E} \equiv \mathcal{E}_{\rm eq}$ and $\mathcal{P} \equiv \mathcal{P}_{\rm eq}$ are the equilibrium energy density and pressure, τ_π and τ_Π are the shear and bulk relaxation time, and $\tau_{\pi\pi}$ is the shear-shear-coupling transport coefficient. The various notations used are

$$\begin{aligned} d_\mu u^\nu &\equiv \partial_\mu u^\nu + \Gamma^\nu_{\mu\alpha}u^\alpha\,, & \sigma^{\mu\nu} &\equiv \nabla^{\langle\mu}u^{\nu\rangle}\,, \\ D_u &\equiv u_\mu d^\mu\,, & A^{\langle\mu\nu\rangle} &\equiv \Delta^{\mu\nu}_{\alpha\beta}A^{\alpha\beta}\,, \\ \theta_u &\equiv \nabla_\mu u^\mu\,, & \Delta^{\mu\nu}_{\alpha\beta} &\equiv \frac{1}{2}\Big(\Delta^\mu_\alpha\Delta^\nu_\beta + \Delta^\mu_\beta\Delta^\nu_\alpha - \frac{2}{3}\Delta^{\mu\nu}\Delta_{\alpha\beta}\Big)\,, \\ \nabla^\mu &\equiv \Delta^{\mu\nu}d_\nu\,, & \omega^{\mu\nu} &\equiv \frac{1}{2}(\nabla^\mu u^\nu - \nabla^\nu u^\mu)\,. \end{aligned} \tag{C5}$$

The non-vanishing Christoffel symbols for polar Milne coordinates are $\Gamma^\tau_{\varsigma\varsigma} = \tau$, $\Gamma^\varsigma_{\varsigma\tau} = 1/\tau$, $\Gamma^r_{\phi\phi} = -r$, and $\Gamma^\phi_{r\phi} = 1/r$. Also, we note that for the smooth initial conditions considered herein in 1+1d, the vorticity tensor vanishes. As shown in Ref. [86], the terms $\varphi_1\Pi^2$, $\varphi_3\pi^{\mu\nu}\pi_{\mu\nu}$, $\varphi_6\Pi\pi^{\mu\nu}$, and $\varphi_7\pi_\alpha^{\langle\mu}\pi^{\nu\rangle\alpha}$ appear only because the collision term is nonlinear in the single-particle distribution function. In the case of the RTA, the collision term is assumed to be linear in the distribution function and one has $\varphi_1 = \varphi_3 = \varphi_6 = \varphi_7 = 0$. In this case, the shear and bulk relaxation times, τ_π and τ_Π, respectively, are equal to the microscopic relaxation time $\tau_{\rm eq}$, i.e., $\tau_\Pi = \tau_\pi = \tau_{\rm eq}$ [33]. The coefficients appearing in the equation for the bulk and shear corrections are [33]

$$\begin{aligned} \frac{\zeta}{\tau_\Pi} &= \left(\frac{1}{3} - c_s^2\right)(\mathcal{E}+\mathcal{P}) - \frac{2}{9}(\mathcal{E}-3\mathcal{P})\,, & \frac{\eta}{\tau_\pi} &= \frac{4}{5}\mathcal{P} + \frac{1}{15}(\mathcal{E}-3\mathcal{P})\,, & \frac{\tau_{\pi\pi}}{\tau_\pi} &= \frac{10}{7}\,, \\ \frac{\delta_{\Pi\Pi}}{\tau_\Pi} &= 1 - c_s^2\,, & \frac{\delta_{\pi\pi}}{\tau_\pi} &= \frac{4}{3}\,, & \frac{\lambda_{\pi\Pi}}{\tau_\pi} &= \frac{6}{5}\,, \\ \frac{\lambda_{\Pi\pi}}{\tau_\Pi} &= \frac{1}{3} - c_s^2\,, \end{aligned} \tag{C6}$$

with $c_s^2 \equiv d\mathcal{P}/d\mathcal{E}$ being the speed of sound squared and $\tau_{\rm eq} = 15\bar{\eta}(\mathcal{E}+\mathcal{P})/(\mathcal{E}+9\mathcal{P})/T$.

1+1d viscous hydrodynamics equations of motion

In the boost-invariant and azimuthally-symmetric case, one has $u^\mu = (u^\tau, u^r, 0, 0)$ and, as a result, $v \equiv \tanh\theta_\perp = u^r/u^\tau$. In addition, for this case, the shear tensor has the following form

$$\pi^{\mu\nu} = \begin{pmatrix} \pi^{\tau\tau} & \pi^{\tau r} & 0 & 0 \\ \pi^{\tau r} & \pi^{rr} & 0 & 0 \\ 0 & 0 & \pi^{\phi\phi} & 0 \\ 0 & 0 & 0 & \pi^{\varsigma\varsigma} \end{pmatrix}. \tag{C7}$$

In this case, expanding Eqs. (C1), (C2), and (C3) in polar Milne coordinates one obtains six equations where only five of them are independent

$$
\begin{aligned}
(\mathcal{E}+\mathcal{P}+\Pi)D_u u^\tau &= -(u^r)^2\Big[\partial_\tau(\mathcal{P}+\Pi) - d_\nu\pi^\nu_\tau\Big] - u^\tau u^r\Big[\partial_r(\mathcal{P}+\Pi) - d_\nu\pi^\nu_r\Big], && \text{(C8)}\\
(\mathcal{E}+\mathcal{P}+\Pi)D_u u^r &= -u^\tau u^r\Big[\partial_\tau(\mathcal{P}+\Pi) - d_\nu\pi^\nu_\tau\Big] - (u^\tau)^2\Big[\partial_r(\mathcal{P}+\Pi) - d_\nu\pi^\nu_r\Big], && \text{(C9)}\\
D_u\mathcal{E} &= -(\mathcal{E}+\mathcal{P}+\Pi)\theta_u - \pi^r_r(1-v^2)^2\nabla^{\langle r}u^{r\rangle} - r^2\,\pi^\phi_\phi\nabla^{\langle\phi}u^{\phi\rangle} - \tau^2\,\pi^\varsigma_\varsigma\nabla^{\langle\varsigma}u^{\varsigma\rangle}, && \text{(C10)}
\end{aligned}
$$

and

$$
\begin{aligned}
\tau_\Pi D_u\Pi + \Pi &= -\zeta\theta_u - \delta_{\Pi\Pi}\Pi\theta_u - \lambda_{\Pi\pi}\Big[2r^2\pi^\phi_\phi\nabla^{\langle\phi}u^{\phi\rangle} + 2\tau^2\pi^\varsigma_\varsigma\nabla^{\langle\varsigma}u^{\varsigma\rangle}\\
&\quad + r^2\pi^\varsigma_\varsigma\nabla^{\langle\phi}u^{\phi\rangle} + \tau^2\pi^\phi_\phi\nabla^{\langle\varsigma}u^{\varsigma\rangle}\Big]\,, && \text{(C11)}\\
\tau_\pi D_u\pi^\phi_\phi + \pi^\phi_\phi &= -2r^2\eta\nabla^{\langle\phi}u^{\phi\rangle} - \delta_{\pi\pi}\pi^\phi_\phi\theta_u - \frac{\tau_{\pi\pi}}{3}\Big[-r^2\pi^\phi_\phi\nabla^{\langle\phi}u^{\phi\rangle} + 2\tau^2\pi^\varsigma_\varsigma\nabla^{\langle\varsigma}u^{\varsigma\rangle}\\
&\quad + r^2\pi^\varsigma_\varsigma\nabla^{\langle\phi}u^{\phi\rangle} + \tau^2\pi^\phi_\phi\nabla^{\langle\varsigma}u^{\varsigma\rangle}\Big] - r^2\lambda_{\pi\Pi}\Pi\nabla^{\langle\phi}u^{\phi\rangle}\,, && \text{(C12)}\\
\tau_\pi D_u\pi^\varsigma_\varsigma + \pi^\varsigma_\varsigma &= -2\tau^2\eta\nabla^{\langle\varsigma}u^{\varsigma\rangle} - \delta_{\pi\pi}\pi^\varsigma_\varsigma\theta_u - \frac{\tau_{\pi\pi}}{3}\Big[2r^2\pi^\phi_\phi\nabla^{\langle\phi}u^{\phi\rangle} - \tau^2\pi^\varsigma_\varsigma\nabla^{\langle\varsigma}u^{\varsigma\rangle}\\
&\quad + r^2\pi^\varsigma_\varsigma\nabla^{\langle\phi}u^{\phi\rangle} + \tau^2\pi^\phi_\phi\nabla^{\langle\varsigma}u^{\varsigma\rangle}\Big] - \tau^2\lambda_{\pi\Pi}\Pi\nabla^{\langle\varsigma}u^{\varsigma\rangle}\,, && \text{(C13)}
\end{aligned}
$$

where

$$
\begin{aligned}
-d_\nu\pi^\nu_\tau &= v^2\partial_\tau\pi^r_r + v\partial_r\pi^r_r + \pi^r_r\Big[\partial_\tau v^2 + \partial_r v + \frac{v^2}{\tau} + \frac{v}{r}\Big] + \frac{1}{\tau}\pi^\varsigma_\varsigma\,, && \text{(C14)}\\
d_\nu\pi^\nu_r &= v\,\partial_\tau\pi^r_r + \partial_r\pi^r_r + \pi^r_r\Big[\partial_\tau v + \frac{v}{\tau} + \frac{2-v^2}{r}\Big] + \frac{1}{r}\pi^\varsigma_\varsigma\,. && \text{(C15)}
\end{aligned}
$$

In addition, one needs the following identities

$$
\begin{aligned}
\nabla^{\langle r}u^{r\rangle} &= -\partial_r u^r - u^r D_u u^r + \frac{1}{3}(u^\tau)^2\theta_u\,, && \text{(C16)}\\
r^2\nabla^{\langle\phi}u^{\phi\rangle} &= -\frac{u^r}{r} + \frac{1}{3}\theta_u\,, && \text{(C17)}\\
\tau^2\nabla^{\langle\varsigma}u^{\varsigma\rangle} &= -\frac{u^\tau}{\tau} + \frac{1}{3}\theta_u\,, && \text{(C18)}\\
\theta_u \equiv \nabla_\alpha u^\alpha &= d_\alpha u^\alpha = \partial_\tau u^\tau + \partial_r u^r + \frac{u^\tau}{\tau} + \frac{u^r}{r}\,, && \text{(C19)}
\end{aligned}
$$

where $\pi^r_\tau = -v\,\pi^r_r$ and $\pi^\phi_\phi = -\pi^\varsigma_\varsigma - (1-v^2)\pi^r_r$ which are a consequence of the transversality of the shear-stress tensor, $u_\mu\pi^{\mu\nu} = 0$. This system of equations has to be closed by providing an equation of state (EoS), e.g. $\mathcal{P}_{\rm eq} = \mathcal{P}_{\rm eq}(\mathcal{E}_{\rm eq})$.

Viscous hydrodynamics freeze-out

The distribution function on the freeze-out hypersurface can be computed assuming that there is a linear correction to the equilibrium one due to shear and bulk viscosities [87, 88]

$$
f(p,x) = f_{\rm eq}(p,x) + \delta f_{\rm shear}(p,x) + \delta f_{\rm bulk}(p,x)\,, \qquad \text{(C20)}
$$

where

$$
\begin{aligned}
\delta f_{\rm shear}(p,x) &= f_{\rm eq}(1-af_{\rm eq})\frac{p_\mu p_\nu\pi^{\mu\nu}}{2(\mathcal{E}+\mathcal{P})T^2}\,, && \text{(C21)}\\
\delta f_{\rm bulk}(p,x) &= -f_{\rm eq}(1-af_{\rm eq})\left[\frac{m_i^2}{3\,p_\mu u^\mu} - \Big(\frac{1}{3} - c_s^2\Big)p_\mu u^\mu\right]\frac{\Pi}{C_\Pi}\,, && \text{(C22)}
\end{aligned}
$$

with

$$C_\Pi = \frac{1}{3}\sum_{i=1}^{N} m_i^2(2s_i+1)\int \frac{d^3p}{(2\pi)^3 E_i} f_{\rm eq}(1-af_{\rm eq})\left[\frac{m_i^2}{3\,p_\mu u^\mu} - \left(\frac{1}{3}-c_s^2\right)p_\mu u^\mu\right], \tag{C23}$$

where m_i is the hadron mass, s_i is the hadron spin, and N is the number of hadrons included in the freezeout. The components of the four-momentum in polar Milne coordinates are

$$\begin{aligned}
p_\tau &= p_t\cosh\varsigma - p_z\sinh\varsigma = m_\perp\cosh(y-\varsigma)\,,\\
p_r &= p_x\cos\phi + p_y\sin\phi = p_\perp\cos(\phi-\varphi)\,,\\
p_\phi &= -p_x\frac{\sin\phi}{r} + p_y\frac{\cos\phi}{r} = -\frac{p_\perp}{r}\sin(\phi-\varphi)\,,\\
p_\varsigma &= -p_t\frac{\sinh\varsigma}{\tau} + p_z\frac{\cosh\varsigma}{\tau} = \frac{m_\perp}{\tau}\sinh(y-\varsigma)\,.
\end{aligned} \tag{C24}$$

Using Eq. (C7) and expanding $p_\mu p_\nu \pi^{\mu\nu}$ in polar Milne coordinates one has

$$\begin{aligned}
p_\mu p_\nu \pi^{\mu\nu} = &-\left(\frac{\pi^\phi_\phi + \pi^\varsigma_\varsigma}{v^2-1}\right)\Big(m_\perp v\cosh(y-\varsigma) - p_\perp\cos(\phi-\varphi)\Big)^2\\
&- \pi^\phi_\phi p_\perp^2\sin^2(\phi-\varphi) - \pi^\varsigma_\varsigma m_\perp^2\sinh^2(y-\varsigma)\,.
\end{aligned} \tag{C25}$$

Appendix D: Explicit formulas for derivatives

In this section, we introduce the notations used in hydrodynamics dynamical equations. In the case of boost-invariant and azimuthally-symmetric flow one can use the basis vectors presented in Ref. [59] to obtain

$$\begin{aligned}
D_u &= u^\mu\partial_\mu = \cosh\theta_\perp\partial_\tau + \sinh\theta_\perp\partial_r\,, & \theta_u &= \partial_\mu u^\mu = \cosh\theta_\perp\left(\frac{1}{\tau}+\partial_r\theta_\perp\right) + \sinh\theta_\perp\left(\frac{1}{r}+\partial_\tau\theta_\perp\right),\\
D_x &= X^\mu\partial_\mu = \sinh\theta_\perp\partial_\tau + \cosh\theta_\perp\partial_r\,, & \theta_x &= \partial_\mu X^\mu = \sinh\theta_\perp\left(\frac{1}{\tau}+\partial_r\theta_\perp\right) + \cosh\theta_\perp\left(\frac{1}{r}+\partial_\tau\theta_\perp\right),\\
D_y &= Y^\mu\partial_\mu = \frac{1}{r}\partial_\phi\,, & \theta_y &= \partial_\mu Y^\mu = 0\,,\\
D_z &= Z^\mu\partial_\mu = \frac{1}{\tau}\partial_\varsigma\,, & \theta_z &= \partial_\mu Z^\mu = 0\,.
\end{aligned} \tag{D1}$$

Appendix E: special functions

In this section, we provide definitions of the special functions appearing in the body of the text. We start by introducing

$$\mathcal{H}_2(y,z) = \frac{y}{\sqrt{y^2-1}}\left[(z^2+1)\tanh^{-1}\sqrt{\frac{y^2-1}{y^2+z^2}} + \sqrt{(y^2-1)(y^2+z^2)}\right], \tag{E1}$$

$$\mathcal{H}_{2T}(y,z) = \frac{y}{(y^2-1)^{3/2}}\left[\left(z^2+2y^2-1\right)\tanh^{-1}\sqrt{\frac{y^2-1}{y^2+z^2}} - \sqrt{(y^2-1)(y^2+z^2)}\right], \tag{E2}$$

$$\mathcal{H}_{2L}(y,z) = \frac{y^3}{(y^2-1)^{3/2}}\left[\sqrt{(y^2-1)(y^2+z^2)} - (z^2+1)\tanh^{-1}\sqrt{\frac{y^2-1}{y^2+z^2}}\right], \tag{E3}$$

and

$$\mathcal{H}_{2x1}(y,z) = \frac{1}{(y^2-1)}\Big[\frac{2(y^2+z^2)\mathcal{H}_{2L}(y,z)}{(1+z^2)} - y^2\mathcal{H}_{2T}(y,z)\Big], \tag{E4}$$

$$\mathcal{H}_{2x2}(y,z) = \frac{y^2}{(y^2-1)}\Big[2\mathcal{H}_{2L}(y,z) - \mathcal{H}_{2T}(y,z)\Big], \tag{E5}$$

$$\mathcal{H}_{2B}(y,z) \equiv \mathcal{H}_{2T}(y,z) + \frac{\mathcal{H}_{2L}(y,z)}{y^2} = \frac{2}{\sqrt{y^2-1}}\tanh^{-1}\sqrt{\frac{y^2-1}{y^2+z^2}}\,. \tag{E6}$$

Derivatives of these functions satisfy the following relations

$$\begin{aligned}
\frac{\partial\mathcal{H}_2(y,z)}{\partial y} &= \frac{1}{y}\Big[\mathcal{H}_2(y,z)+\mathcal{H}_{2L}(y,z)\Big], &\quad \frac{\partial\mathcal{H}_{2T}(y,z)}{\partial y} &= \frac{1}{y(y^2-1)}\Big[2\mathcal{H}_{2L}(y,z)-\mathcal{H}_{2T}(y,z)\Big],\\
\frac{\partial\mathcal{H}_2(y,z)}{\partial z} &= \frac{1}{z}\Big[\mathcal{H}_2(y,z)-\mathcal{H}_{2L}(y,z)-\mathcal{H}_{2T}(y,z)\Big], &\quad \frac{\partial\mathcal{H}_{2T}(y,z)}{\partial z} &= \frac{-2z}{y^2(1+z^2)}\mathcal{H}_{2L}(y,z).
\end{aligned} \tag{E7}$$

1. Massive Case

The $\mathcal{H}$-functions appearing in definitions of components of the energy-momentum tensor in the massive case are

$$\mathcal{H}_3(\boldsymbol{\alpha},\hat{m}) \equiv \tilde{N}\alpha_x\alpha_y\int_0^{2\pi} d\phi\,\alpha_\perp^2\int_0^\infty d\hat{p}\,\hat{p}^3 f_{\rm eq}\Big(\sqrt{\hat{p}^2+\hat{m}^2}\Big)\,\mathcal{H}_2\left(\frac{\alpha_z}{\alpha_\perp},\frac{\hat{m}}{\alpha_\perp\hat{p}}\right), \tag{E8}$$

$$\mathcal{H}_{3x}(\boldsymbol{\alpha},\hat{m}) \equiv \tilde{N}\alpha_x^3\alpha_y\int_0^{2\pi} d\phi\,\cos^2\phi\int_0^\infty d\hat{p}\,\hat{p}^3 f_{\rm eq}\Big(\sqrt{\hat{p}^2+\hat{m}^2}\Big)\,\mathcal{H}_{2T}\left(\frac{\alpha_z}{\alpha_\perp},\frac{\hat{m}}{\alpha_\perp\hat{p}}\right), \tag{E9}$$

$$\mathcal{H}_{3y}(\boldsymbol{\alpha},\hat{m}) \equiv \tilde{N}\alpha_x\alpha_y^3\int_0^{2\pi} d\phi\,\sin^2\phi\int_0^\infty d\hat{p}\,\hat{p}^3 f_{\rm eq}\Big(\sqrt{\hat{p}^2+\hat{m}^2}\Big)\,\mathcal{H}_{2T}\left(\frac{\alpha_z}{\alpha_\perp},\frac{\hat{m}}{\alpha_\perp\hat{p}}\right), \tag{E10}$$

$$\mathcal{H}_{3T}(\boldsymbol{\alpha},\hat{m}) \equiv \frac{1}{2}\Big[\mathcal{H}_{3x}(\boldsymbol{\alpha},\hat{m})+\mathcal{H}_{3y}(\boldsymbol{\alpha},\hat{m})\Big], \tag{E11}$$

$$\mathcal{H}_{3L}(\boldsymbol{\alpha},\hat{m}) \equiv \tilde{N}\alpha_x\alpha_y\int_0^{2\pi} d\phi\,\alpha_\perp^2\int_0^\infty d\hat{p}\,\hat{p}^3 f_{\rm eq}\Big(\sqrt{\hat{p}^2+\hat{m}^2}\Big)\,\mathcal{H}_{2L}\left(\frac{\alpha_z}{\alpha_\perp},\frac{\hat{m}}{\alpha_\perp\hat{p}}\right), \tag{E12}$$

$$\mathcal{H}_{3B}(\boldsymbol{\alpha},\hat{m}) \equiv \tilde{N}\alpha_x\alpha_y\int_0^{2\pi} d\phi\int_0^\infty d\hat{p}\,\hat{p} f_{\rm eq}\Big(\sqrt{\hat{p}^2+\hat{m}^2}\Big)\,\mathcal{H}_{\rm 2B}\left(\frac{\alpha_z}{\alpha_\perp},\frac{\hat{m}}{\alpha_\perp\hat{p}}\right), \tag{E13}$$

The relevant derivatives are

$$\begin{aligned}
\frac{\partial\mathcal{H}_3}{\partial\alpha_x} &= \frac{1}{\alpha_x}(\mathcal{H}_3+\mathcal{H}_{3x})\,, &\quad \frac{\partial\mathcal{H}_{3x}}{\partial\alpha_x} &= \frac{1}{\alpha_x}(3\mathcal{H}_{3x}-\mathcal{H}_{3x1})\,,\\
\frac{\partial\mathcal{H}_3}{\partial\alpha_y} &= \frac{1}{\alpha_y}(\mathcal{H}_3+\mathcal{H}_{3y})\,, &\quad \frac{\partial\mathcal{H}_{3x}}{\partial\alpha_y} &= \frac{1}{\alpha_y}(\mathcal{H}_{3x}-\mathcal{H}_{3x2})\,,\\
\frac{\partial\mathcal{H}_3}{\partial\alpha_z} &= \frac{1}{\alpha_z}(\mathcal{H}_3+\mathcal{H}_{3L})\,, &\quad \frac{\partial\mathcal{H}_{3x}}{\partial\alpha_z} &= \frac{1}{\alpha_z}\mathcal{H}_{3x3}\,,\\
\frac{\partial\mathcal{H}_3}{\partial\hat{m}} &= \frac{1}{\hat{m}}(\mathcal{H}_3-\mathcal{H}_{3L}-2\mathcal{H}_{3T}-\mathcal{H}_{3m})\,, &\quad \frac{\partial\mathcal{H}_{3x}}{\partial\hat{m}} &= \frac{1}{\hat{m}}(\mathcal{H}_{3m1}-\mathcal{H}_{3m2})\,,
\end{aligned} \tag{E14}$$

with

$$\mathcal{H}_{3x1}(\boldsymbol{\alpha},\hat{m}) \equiv \tilde{N}\frac{\alpha_x^5\alpha_y}{\alpha_z^2}\int_0^{2\pi} d\phi\,\cos^4\phi\int_0^\infty d\hat{p}\,\hat{p}^3 f_{\rm eq}\Big(\sqrt{\hat{p}^2+\hat{m}^2}\Big)\,\mathcal{H}_{2x1}\left(\frac{\alpha_z}{\alpha_\perp},\frac{\hat{m}}{\alpha_\perp\hat{p}}\right), \tag{E15}$$

$$\mathcal{H}_{3x2}(\boldsymbol{\alpha},\hat{m}) \equiv \tilde{N}\frac{\alpha_x^3\alpha_y^3}{\alpha_z^2}\int_0^{2\pi} d\phi\,\cos^2\phi\sin^2\phi\int_0^\infty d\hat{p}\,\hat{p}^3 f_{\rm eq}\Big(\sqrt{\hat{p}^2+\hat{m}^2}\Big)\,\mathcal{H}_{2x1}\left(\frac{\alpha_z}{\alpha_\perp},\frac{\hat{m}}{\alpha_\perp\hat{p}}\right), \tag{E16}$$

$$\mathcal{H}_{3x3}(\boldsymbol{\alpha},\hat{m}) \equiv \tilde{N}\frac{\alpha_x^3\alpha_y}{\alpha_z^2}\int_0^{2\pi} d\phi\,\alpha_\perp^2\,\cos^2\phi\int_0^\infty d\hat{p}\,\hat{p}^3 f_{\rm eq}\Big(\sqrt{\hat{p}^2+\hat{m}^2}\Big)\,\mathcal{H}_{2x2}\left(\frac{\alpha_z}{\alpha_\perp},\frac{\hat{m}}{\alpha_\perp\hat{p}}\right), \tag{E17}$$

$$\mathcal{H}_{3m}(\boldsymbol{\alpha},\hat{m}) \equiv \tilde{N}\alpha_x\alpha_y\hat{m}^2 \int_0^{2\pi} d\phi\,\alpha_\perp^2 \int_0^\infty d\hat{p}\,\hat{p}^3 \frac{f_{\rm eq}\left(\sqrt{\hat{p}^2+\hat{m}^2}\right)}{\sqrt{\hat{p}^2+\hat{m}^2}} \mathcal{H}_2\left(\frac{\alpha_z}{\alpha_\perp},\frac{\hat{m}}{\alpha_\perp\hat{p}}\right), \tag{E18}$$

$$\mathcal{H}_{3m1}(\boldsymbol{\alpha},\hat{m}) \equiv \mathcal{H}_{3x1}(\boldsymbol{\alpha},\hat{m}) + \mathcal{H}_{3x2}(\boldsymbol{\alpha},\hat{m}) - \mathcal{H}_{3x3}(\boldsymbol{\alpha},\hat{m}), \tag{E19}$$

$$\mathcal{H}_{3m2}(\boldsymbol{\alpha},\hat{m}) \equiv \tilde{N}\alpha_x^3\alpha_y\hat{m}^2 \int_0^{2\pi} d\phi\,\cos^2\phi \int_0^\infty d\hat{p}\,\hat{p}^3 \frac{f_{\rm eq}\left(\sqrt{\hat{p}^2+\hat{m}^2}\right)}{\sqrt{\hat{p}^2+\hat{m}^2}} \mathcal{H}_{2T}\left(\frac{\alpha_z}{\alpha_\perp},\frac{\hat{m}}{\alpha_\perp\hat{p}}\right), \tag{E20}$$

where $\alpha_\perp^2 \equiv \alpha_x^2\cos^2\phi + \alpha_y^2\sin^2\phi$.

2. Massless Case

The $\hat{\mathcal{H}}$-functions used in definition of bulk variables in the standard (massless) case are

$$\hat{\mathcal{H}}_3(\boldsymbol{\alpha}) \equiv \frac{1}{24\pi\tilde{N}} \lim_{m\to 0} \mathcal{H}_3(\boldsymbol{\alpha},\hat{m}) = \frac{1}{4\pi}\alpha_x\alpha_y \int_0^{2\pi} d\phi\,\alpha_\perp^2 \bar{\mathcal{H}}_2\left(\frac{\alpha_z}{\alpha_\perp}\right), \tag{E21}$$

$$\hat{\mathcal{H}}_{3x}(\boldsymbol{\alpha}) \equiv \frac{1}{8\pi\tilde{N}} \lim_{m\to 0} \mathcal{H}_{3x}(\boldsymbol{\alpha},\hat{m}) = \frac{3}{4\pi}\alpha_x^3\alpha_y \int_0^{2\pi} d\phi\,\cos^2\phi\, \bar{\mathcal{H}}_{2T}\left(\frac{\alpha_z}{\alpha_\perp}\right), \tag{E22}$$

$$\hat{\mathcal{H}}_{3y}(\boldsymbol{\alpha}) \equiv \frac{1}{8\pi\tilde{N}} \lim_{m\to 0} \mathcal{H}_{3y}(\boldsymbol{\alpha},\hat{m}) = \frac{3}{4\pi}\alpha_x\alpha_y^3 \int_0^{2\pi} d\phi\,\sin^2\phi\, \bar{\mathcal{H}}_{2T}\left(\frac{\alpha_z}{\alpha_\perp}\right), \tag{E23}$$

$$\hat{\mathcal{H}}_{3L}(\boldsymbol{\alpha}) \equiv \frac{1}{8\pi\tilde{N}} \lim_{m\to 0} \mathcal{H}_{3L}(\boldsymbol{\alpha},\hat{m}) = \frac{3}{4\pi}\alpha_x\alpha_y \int_0^{2\pi} d\phi\,\alpha_\perp^2 \bar{\mathcal{H}}_{2L}\left(\frac{\alpha_z}{\alpha_\perp}\right), \tag{E24}$$

where $\bar{\mathcal{H}}_{2,2T,2L}(y) \equiv \mathcal{H}_{2,2T,2L}(y,0)$.

[1] P. Huovinen, P. F. Kolb, U. W. Heinz, P. V. Ruuskanen, and S. A. Voloshin, Phys. Lett. **B503**, 58 (2001), arXiv:hep-ph/0101136.

[2] T. Hirano and K. Tsuda, Phys. Rev. **C66**, 054905 (2002), arXiv:nucl-th/0205043.

[3] P. F. Kolb and U. W. Heinz, In Hwa, R.C. (ed.) et al.: Quark gluon plasma , 634 (2003), arXiv:nucl-th/0305084.

[4] A. Muronga, Phys. Rev. Lett. **88**, 062302 (2002), arXiv:nucl-th/0104064.

[5] A. Muronga, Phys. Rev. **C69**, 034903 (2004), arXiv:nucl-th/0309055.

[6] A. Muronga and D. H. Rischke, (2004), arXiv:nucl-th/0407114 [nucl-th].

[7] U. W. Heinz, H. Song, and A. K. Chaudhuri, Phys.Rev. **C73**, 034904 (2006), arXiv:nucl-th/0510014 [nucl-th].

[8] R. Baier, P. Romatschke, and U. A. Wiedemann, Phys.Rev. **C73**, 064903 (2006), arXiv:hep-ph/0602249 [hep-ph].

[9] P. Romatschke and U. Romatschke, Phys. Rev. Lett. **99**, 172301 (2007), arXiv:0706.1522 [nucl-th].

[10] R. Baier, P. Romatschke, D. T. Son, A. O. Starinets, and M. A. Stephanov, JHEP **0804**, 100 (2008), arXiv:0712.2451 [hep-th].

[11] K. Dusling and D. Teaney, Phys. Rev. **C77**, 034905 (2008), arXiv:0710.5932 [nucl-th].

[12] M. Luzum and P. Romatschke, Phys. Rev. **C78**, 034915 (2008), arXiv:0804.4015 [nucl-th].

[13] H. Song and U. W. Heinz, J.Phys.G **G36**, 064033 (2009), arXiv:0812.4274 [nucl-th].

[14] U. W. Heinz, Relativistic Heavy Ion Physics, Landolt-Boernstein New Series, I/23, edited by R. Stock, Springer Verlag, New York, Chap. 5 (2010), arXiv:0901.4355 [nucl-th].

[15] P. Bozek and I. Wyskiel, Phys.Rev. **C79**, 044916 (2009), arXiv:0902.4121 [nucl-th].

[16] P. Bozek, Phys.Rev. **C81**, 034909 (2010), arXiv:0911.2397 [nucl-th].

[17] A. El, Z. Xu, and C. Greiner, Phys. Rev. **C81**, 041901 (2010), arXiv:0907.4500 [hep-ph].

[18] J. Peralta-Ramos and E. Calzetta, Phys. Rev. **D80**, 126002 (2009), arXiv:0908.2646 [hep-ph].

[19] J. Peralta-Ramos and E. Calzetta, Phys.Rev. **C82**, 054905 (2010), arXiv:1003.1091 [hep-ph].

[20] G. Denicol, T. Kodama, and T. Koide, J.Phys.G **G37**, 094040 (2010), arXiv:1002.2394 [nucl-th].

[21] G. Denicol, T. Koide, and D. Rischke, Phys.Rev.Lett. **105**, 162501 (2010), arXiv:1004.5013 [nucl-th].

[22] B. Schenke, S. Jeon, and C. Gale, Phys.Rev.Lett. **106**, 042301 (2011), arXiv:1009.3244 [hep-ph].

[23] B. Schenke, S. Jeon, and C. Gale, Phys.Lett. **B702**, 59 (2011), arXiv:1102.0575 [hep-ph].

[24] P. Bozek, Phys.Lett. **B699**, 283 (2011), arXiv:1101.1791 [nucl-th].

[25] P. Bozek, Phys.Rev. **C85**, 034901 (2012), arXiv:1110.6742 [nucl-th].

[26] H. Niemi, G. S. Denicol, P. Huovinen, E. Molnár, and D. H. Rischke, Phys.Rev.Lett. **106**, 212302 (2011), arXiv:1101.2442 [nucl-th].

[27] H. Niemi, G. S. Denicol, P. Huovinen, E. Molnár, and D. H. Rischke, Phys. Rev. C **86**, 014909 (2012).

[28] P. Bożek and I. Wyskiel-Piekarska, Phys. Rev. C **85**, 064915 (2012).

[29] G. S. Denicol, H. Niemi, E. Molnár, and D. H. Rischke, Phys. Rev. D **85**, 114047 (2012).

[30] G. Denicol, E. Molnár, H. Niemi, and D. Rischke, Eur. Phys. J. A **48**, 170 (2012), arXiv:1206.1554 [nucl-th].

[31] J. Peralta-Ramos and E. Calzetta, Phys.Rev. **D87**, 034003 (2013), arXiv:1212.0824 [nucl-th].

[32] E. Calzetta, Phys. Rev. **D92**, 045035 (2015), arXiv:1402.5278 [hep-ph].

[33] G. S. Denicol, S. Jeon, and C. Gale, Phys. Rev. **C90**, 024912 (2014), arXiv:1403.0962 [nucl-th].

[34] W. Florkowski, A. Jaiswal, E. Maksymiuk, R. Ryblewski, and M. Strickland, Phys. Rev. **C91**, 054907 (2015), arXiv:1503.03226 [nucl-th].

[35] S. Ryu, J. F. Paquet, C. Shen, G. S. Denicol, B. Schenke, S. Jeon, and C. Gale, Phys. Rev. Lett. **115**, 132301 (2015), arXiv:1502.01675 [nucl-th].

[36] H. Niemi, K. J. Eskola, R. Paatelainen, and K. Tuominen, Phys. Rev. **C93**, 014912 (2016), arXiv:1511.04296 [hep-ph].

[37] H. Niemi, K. J. Eskola, R. Paatelainen, and K. Tuominen (2015) arXiv:1512.05132 [hep-ph].

[38] M. Martinez and M. Strickland, Nucl. Phys. **A848**, 183 (2010), arXiv:1007.0889 [nucl-th].

[39] W. Florkowski and R. Ryblewski, Phys.Rev. **C83**, 034907 (2011), arXiv:1007.0130 [nucl-th].

[40] R. Ryblewski and W. Florkowski, J.Phys.G **G38**, 015104 (2011), arXiv:1007.4662 [nucl-th].

[41] M. Martinez and M. Strickland, Nucl.Phys. **A856**, 68 (2011), arXiv:1011.3056 [nucl-th].

[42] R. Ryblewski and W. Florkowski, Eur.Phys.J. **C71**, 1761 (2011), arXiv:1103.1260 [nucl-th].

[43] W. Florkowski and R. Ryblewski, Phys.Rev. **C85**, 044902 (2012), arXiv:1111.5997 [nucl-th].

[44] M. Martinez, R. Ryblewski, and M. Strickland, Phys.Rev. **C85**, 064913 (2012), arXiv:1204.1473 [nucl-th].

[45] R. Ryblewski and W. Florkowski, Phys. Rev. **C85**, 064901 (2012), arXiv:1204.2624 [nucl-th].

[46] W. Florkowski, R. Maj, R. Ryblewski, and M. Strickland, Phys.Rev. **C87**, 034914 (2013), arXiv:1209.3671 [nucl-th].

[47] W. Florkowski and R. Maj, Acta Phys.Polon. **B44**, 2003 (2013), arXiv:1309.2786 [nucl-th].

[48] R. Ryblewski, J.Phys. **G40**, 093101 (2013).

[49] D. Bazow, U. W. Heinz, and M. Strickland, Phys.Rev. **C90**, 054910 (2014), arXiv:1311.6720 [nucl-th].

[50] L. Tinti and W. Florkowski, Phys.Rev. **C89**, 034907 (2014), arXiv:1312.6614 [nucl-th].

[51] W. Florkowski, R. Ryblewski, M. Strickland, and L. Tinti, Phys.Rev. **C89**, 054909 (2014), arXiv:1403.1223 [hep-ph].

[52] W. Florkowski and O. Madetko, Acta Phys.Polon. **B45**, 1103 (2014), arXiv:1402.2401 [nucl-th].

[53] M. Nopoush, R. Ryblewski, and M. Strickland, Phys.Rev. **C90**, 014908 (2014), arXiv:1405.1355 [hep-ph].

[54] G. S. Denicol, W. Florkowski, R. Ryblewski, and M. Strickland, Phys.Rev. **C90**, 044905 (2014), arXiv:1407.4767 [hep-ph].

[55] L. Tinti, R. Ryblewski, W. Florkowski, and M. Strickland, Nucl. Phys. **A946**, 29 (2016), arXiv:1505.06456 [hep-ph].

[56] D. Bazow, U. W. Heinz, and M. Martinez, Phys.Rev. **C91**, 064903 (2015), arXiv:1503.07443 [nucl-th].

[57] M. Nopoush, M. Strickland, R. Ryblewski, D. Bazow, U. Heinz, and M. Martinez, Phys. Rev. **C92**, 044912 (2015), arXiv:1506.05278 [nucl-th].

[58] D. Bazow, M. Martinez, and U. W. Heinz, Phys. Rev. **D93**, 034002 (2016), [Phys. Rev.D93,034002(2016)], arXiv:1507.06595 [nucl-th].

[59] M. Alqahtani, M. Nopoush, and M. Strickland, Phys. Rev. **C92**, 054910 (2015), arXiv:1509.02913 [hep-ph].

[60] W. Florkowski, E. Maksymiuk, R. Ryblewski, and L. Tinti, Phys. Rev. **C92**, 054912 (2015), arXiv:1508.04534 [nucl-th].

[61] E. Molnar, H. Niemi, and D. H. Rischke, (2016), arXiv:1602.00573 [nucl-th].

[62] M. Strickland, Acta Phys. Polon. **B45**, 2355 (2014), arXiv:1410.5786 [nucl-th].

[63] W. Florkowski, R. Ryblewski, and M. Strickland, Nucl. Phys. **A916**, 249 (2013), arXiv:1304.0665 [nucl-th].

[64] W. Florkowski, R. Ryblewski, and M. Strickland, Phys. Rev. **C88**, 024903 (2013), arXiv:1305.7234 [nucl-th].

[65] W. Florkowski, E. Maksymiuk, R. Ryblewski, and M. Strickland, Phys. Rev. **C89**, 054908 (2014), arXiv:1402.7348 [hep-ph].

[66] M. Nopoush, R. Ryblewski, and M. Strickland, Phys. Rev. **D91**, 045007 (2015), arXiv:1410.6790 [nucl-th].

[67] G. S. Denicol, U. W. Heinz, M. Martinez, J. Noronha, and M. Strickland, Phys. Rev. Lett. **113**, 202301 (2014), arXiv:1408.5646 [hep-ph].

[68] G. S. Denicol, U. W. Heinz, M. Martinez, J. Noronha, and M. Strickland, Phys. Rev. **D90**, 125026 (2014), arXiv:1408.7048 [hep-ph].

[69] M. Bluhm and T. Schaefer, Phys. Rev. Lett. **116**, 115301 (2016), arXiv:1512.00862 [cond-mat.quant-gas].

[70] M. Bluhm and T. Schaefer, Phys. Rev. **A92**, 043602 (2015), arXiv:1505.00846 [cond-mat.quant-gas].

[71] H. A. Weldon, Phys. Rev. **D26**, 1394 (1982).

[72] H. A. Weldon, Phys. Rev. **D26**, 2789 (1982).

[73] E. Braaten and R. D. Pisarski, Nucl. Phys. **B337**, 569 (1990).

[74] J.-P. Blaizot and E. Iancu, Phys. Rept. **359**, 355 (2002), arXiv:hep-ph/0101103 [hep-ph].

[75] J. O. Andersen, E. Braaten, and M. Strickland, Phys. Rev. Lett. **83**, 2139 (1999), arXiv:hep-ph/9902327 [hep-ph].

[76] J. O. Andersen, E. Petitgirard, and M. Strickland, Phys.Rev. **D70**, 045001 (2004), arXiv:hep-ph/0302069 [hep-ph].

[77] J. O. Andersen and M. Strickland, Annals Phys. **317**, 281 (2005), arXiv:hep-ph/0404164 [hep-ph].

[78] J. O. Andersen, L. E. Leganger, M. Strickland, and N. Su, JHEP **08**, 053 (2011), arXiv:1103.2528 [hep-ph].

[79] N. Haque, A. Bandyopadhyay, J. O. Andersen, M. G. Mustafa, M. Strickland, and N. Su, JHEP **05**, 027 (2014), arXiv:1402.6907 [hep-ph].

[80] S. Borsanyi, G. Endrodi, Z. Fodor, A. Jakovac, S. D. Katz, *et al.*, JHEP **1011**, 077 (2010), arXiv:1007.2580

[hep-lat].
[81] M. I. Gorenstein and S. N. Yang, Physical Review D **52**, 5206 (1995).
[82] G. Torrieri, S. Steinke, W. Broniowski, W. Florkowski, J. Letessier, and J. Rafelski, Comput. Phys. Commun. **167**, 229 (2005), arXiv:nucl-th/0404083 [nucl-th].
[83] G. Torrieri, S. Jeon, J. Letessier, and J. Rafelski, Comput. Phys. Commun. **175**, 635 (2006), arXiv:nucl-th/0603026 [nucl-th].
[84] M. Petran, J. Letessier, J. Rafelski, and G. Torrieri, Comput. Phys. Commun. **185**, 2056 (2014), arXiv:1310.5108 [hep-ph].
[85] G. Denicol and B. Schenke, private communication (2016).
[86] E. Molnr, H. Niemi, G. S. Denicol, and D. H. Rischke, Phys. Rev. **D89**, 074010 (2014), arXiv:1308.0785 [nucl-th].
[87] J.-B. Rose, J.-F. Paquet, G. S. Denicol, M. Luzum, B. Schenke, S. Jeon, and C. Gale, *Proceedings, 24th International Conference on Ultra-Relativistic Nucleus-Nucleus Collisions (Quark Matter 2014)*, Nucl. Phys. **A931**, 926 (2014), arXiv:1408.0024 [nucl-th].
[88] D. Teaney, Phys. Rev. **C68**, 034913 (2003), arXiv:nucl-th/0301099 [nucl-th].